Reconstruction of the Hubble Space Telescope mirror figure from out-of-focus stellar images

C. Roddier and F. Roddier

Institute for Astronomy, University of Hawaii
2680 Woodlawn Drive, Honolulu, HI 96822

ABSTRACT

From the illumination recorded in two defocused stellar images it is possible to reconstruct both the amplitude and the phase of the incoming wave front viewed from the focal plane, providing a powerful diagnostic tool for telescope optics. We present here results obtained from defocused stellar images taken in flight by the Hubble Space Telescope.

1. INTRODUCTION

The observation of defocused stellar images has long been known as a sensitive test for mirror figure errors. However there have been few attempts to extract quantitative information from such images. Recently we proposed a method based on geometrical optics and only valid for highly defocused images [1]. It consists of taking the difference in illumination between two defocused images as a map of the local wavefront Laplacian. The wave front is reconstructed by solving a Poisson equation. The method is comparable in sensitivity to a Hartmann test [2] and has been successfully applied to control the optical quality of telescopes on Mauna Kea [3]. Because it is based on the geometrical optics approximation, the method works with broad-band, extended light sources such as stellar sources blurred by atmospheric turbulence.

In the framework of the Hubble Aberration Recovery Program (HARP) organized by the Jet Propulsion Laboratory (JPL), we requested that highly defocused images be taken in flight by the Hubble Space Telescope (HST) so that the method could be applied to estimate the exact amount of spherical aberration. However, because defocusing the image also defocus the telescope tracking system, it was not possible to obtain images sufficiently defocused for the method to apply. In the defocused images recorded by the HST, diffraction effects dominate and the geometrical optics approximation becomes inaccurate. Direct inversion is not possible, but iterative phase retrieval algorithms can still be used to recover the wavefront amplitude and phase.

The first practical phase retrieval algorithm was described by Gershberg and Saxton [4]. This algorithm uses a single in-focus image rather than two defocused images. In addition the pupil transmission function is assumed to be known. One starts with a first guess of the incoming wavefront phase (which can be random) and computes the diffracted amplitude and phase in the image plane by taking the Fourier transform of the input complex wavefront. The calculated amplitude is then replaced by the observed amplitude (square root of the image intensity). An inverse Fourier transform gives a new estimate of the incoming wavefront phase and amplitude. The calculated amplitude is again replaced by the known incoming wavefront amplitude (given by the pupil transmission function) and the process is iterated. At each step the difference between the known amplitude and the calculated amplitude gives a measure of the current error. Iteration is stopped when the error drops below an acceptable level.

The algorithm first quickly converges but then tends to stagnate. Further more, the solution may not be always unique. Fienup et al. [5] developed methods to avoid stagnation and applied the technique to reconstruct images from the modulus of their Fourier transform. Misell [6-8] found that by using both an in-focus image and an out-of-focus image, ambiguities can be removed and better convergence can be achieved. The Misell algorithm is now used to test millimetric radio antennas [9,10]. As the Gershberg-Saxton algorithm, the Misell algorithm starts with a first guess for the complex wavefront in the telescope entrance pupil and computes the complex amplitude associated with the in-focus image. The calculated amplitude is replaced by the observed amplitude and the result is Fourier transformed back producing a new estimate of the complex amplitude in the telescope pupil plane. However no constraint is applied in the pupil plane other than setting to zero any value outside the pupil. The complex amplitude in the pupil plane is multiplied by a quadratic phase factor, which introduces a defocus, and a new Fourier transform is taken giving and estimate of the complex amplitude in the defocused image. Again the computed amplitude is replaced by the observed amplitude and the result is Fourier transformed back. The process is then iterated.

 0-8194-0603-1/91/$4.00

We present here results obtained by applying a modified Misell-type algorithm to HST data.

2. ALGORITHM

From our previous experience in reconstructing wavefronts it was clear that highly defocused images were still necessary to retrieve the wave front with a good spatial resolution. This is because highly defocused images make a better use of the detector dynamic range, can be used with a larger optical bandwidth, and are less sensitive to telescope jitter. In the Misell algorithm, the complex amplitude in a defocused image is computed by multiplying the complex amplitude in the pupil plane by a quadratic phase factor and taking the Fourier transform of the product. However, when the amount of required defocus is large, the associated phase factor may become under sampled producing aliasing errors. Another possible approach is to take the Fourier transform of the complex wavefront first, multiply the result by a defocus phase factor and Fourier transform back. This second approach gives better results for highly defocused images but it requires the use of two fast Fourier transforms (FFT) instead of one. In the case of the HST, the phase of the wavefront in the pupil plane is affected by spherical aberration. Adding a defocus term may partially balance the spherical aberration producing a least confusion image beyond the paraxial focus. When this happen, the phase can still be properly sampled in the pupil plane and the complex amplitude in the defocused image can be computed with a single Fourier transform. For defocused images taken before the paraxial focus, adding a defocus term increases the phase slopes requiring smaller sampling intervals. These considerations led us to modify the Misell algorithm.

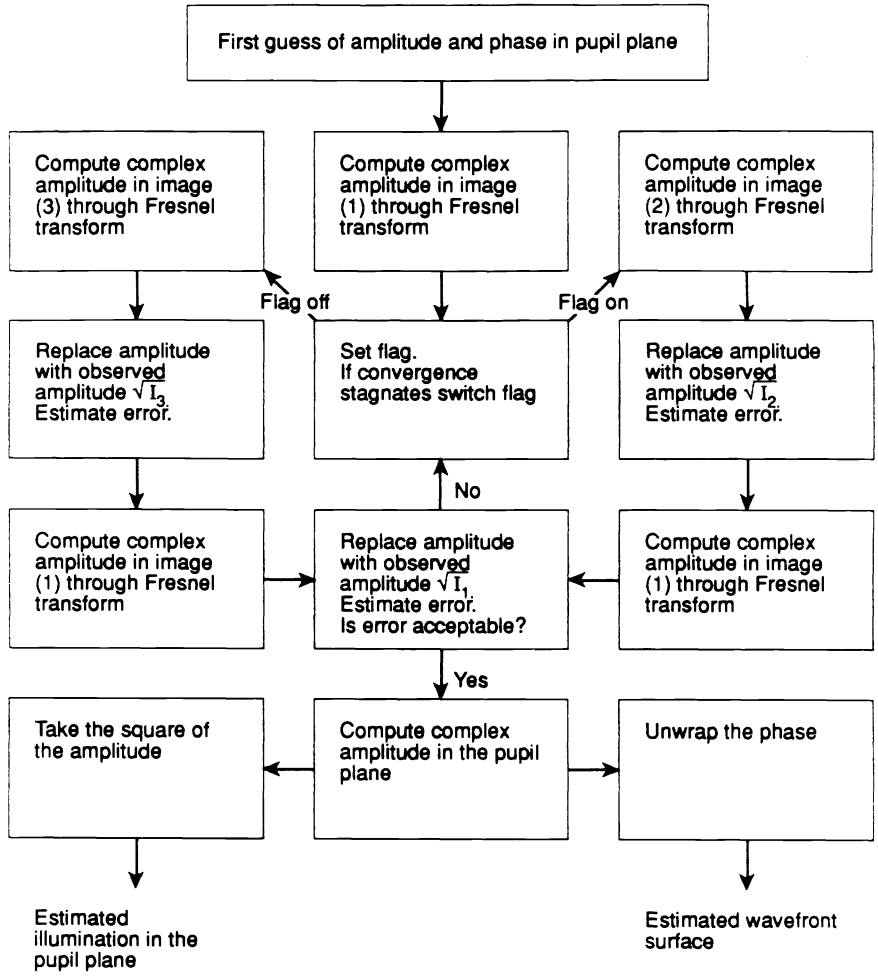

Fig. 1. Flow chart of the phase retrieval algorithm used to process HST images.

The algorithm we used is summarized in Fig. 1. It starts with a first guess of the wavefront aberration (± 0.5 μm) and of the pupil transmission function and computes the complex amplitude for an image (1) recorded beyond the paraxial focus. This can be done by using a single Fourier transform with a defocus factor which is partially balanced by the telescope spherical aberration. The computed amplitude is replaced by the observed amplitude and the result is Fourier transformed back with a different defocus factor producing the complex amplitude in an image (2) taken before the paraxial focus rather than in the pupil plane. Again the computed amplitude is replaced by the observed amplitude and the result is used to compute back the complex amplitude for image (1). The process goes on iterating back and forth between image (1) and image (2) without ever going back to the pupil plane. As for the Gershberg algorithm [11], faster convergence is observed when image (1) is multiplyed by an apodization window. The width of the window is increased at each iteration and then the window is suppressed.

As for any Gershberg-Saxton type algorithm, convergence slows down and stagnates after several iterations. To avoid stagnation, we used the following procedure. We leave out image (2) and use our current estimate of the complex amplitude for image (1) to compute the complex amplitude for a third image (3) using a single Fourier transform with a different defocus factor. The computed amplitude is replaced by the amplitude observed in image (3) and a new series of iteration is done iterating back and forth between image (1) and image (3). Convergence becomes rapid again and then slows down. When it stagnates one switch back to iterations between image (1) and image (2) and so forth. This procedure was found to boost up convergence but was also found to be sensitive to both decentering and despace errors in the three images. Indeed as long as only two images are used a decenter error translates into a wavefront tilt; a despace error translate into a wavefront defocus term. Adding a third image requires perfect alignment and correct despace values otherwise convergence is affected.

A way to control the decenter and despace errors was empirically found by observing the reconstructed pupil amplitude. One start with assumed aberrations and a uniformly illuminated pupil (no central obscuration nor spider arms), and compute the complex amplitude in the image. The amplitude is replaced by the observed amplitude and the result is transformed back to the pupil plane. The central obscuration and the spider arms will appear as darker areas. Decenter errors tend to distort the reconstructed spider arms telling the direction of the decenter. Despace errors tend to produce a non-uniform illumination in the reconstructed pupil intensity. Either the edge or the center of the pupil is brighter depending upon the sign of the despace error.

3. RESULTS

The algorithm described above was thoroughly tested on simulated data and applied to HST images. The results presented here as an example were obtained from a set of three images taken in the same run with the Planetary Camera (PC) at a wavelength of 487 nm. Fig. 2 shows the position of the three images along the aberrated beam. On real data

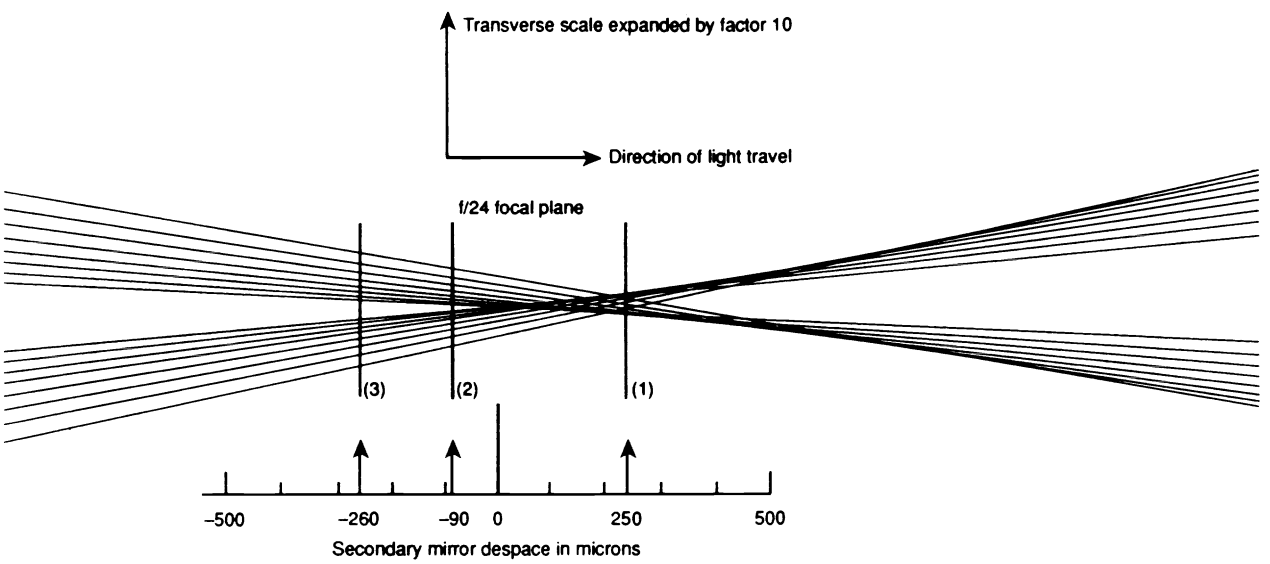

Fig. 2. Ray tracing showing the effect of spherical aberration at the focal plane of the Space Telescope (Courtesy A. Vaughan). The three processed images were taken at the indicated position and obtained by moving the telescope secondary mirror along the optical axis, respectively -260, -90, and +290 μm away from its nominal position.

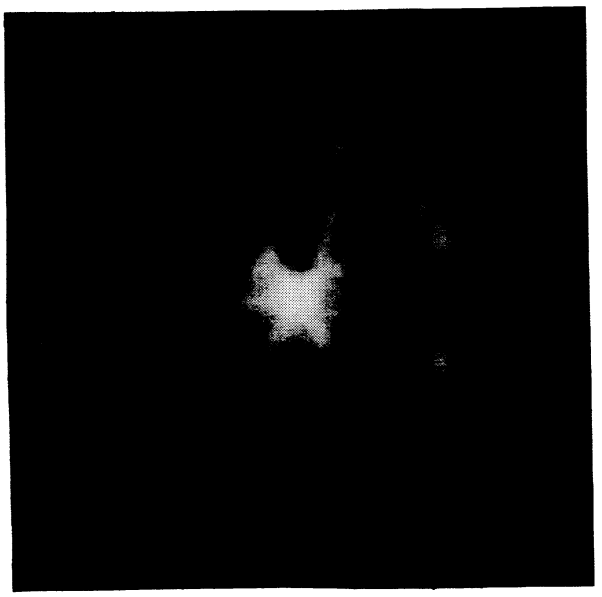

Fig. 3. Image (1) computed from the reconstructed wavefront. The 7.5 μm/pixel sampling is twice that of the observed image.

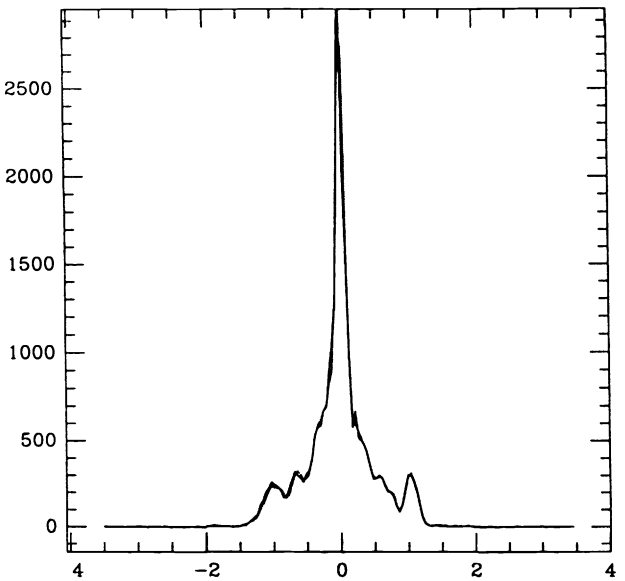

Fig. 4. Photometric profiles across image (1). Full line is the computed image shown in Fig. 3. Dotted line is the actually recorded image.

interpolation is a source of error. With an appropriate choice of the sampling in the pupil plane and of the reference sphere one can always minimize sampling errors in two planes. Interpolation becomes necessary in the third plane. The PC camera has 15 micron pixels. We used 256 x 256 arrays with a telescope pupil size of 65.71 pixels. This gave us computed images with the following sampling: 7.5 micron pixels for the first image (double sampling), 15 micron pixels for the second image (single sampling) and 22.2 micron pixels for the third image. As a result comparison with the observed image required interpolation only for the third image.

Several runs were made using slightly different initial guesses and varying the order of iterations. In each case an estimate of the complex amplitude in the telescope pupil plane was obtained. All the results were quite similar.

Fig. 5. Image (2) as recorded by the Space Telescope. The sampling is the original 15 μm/pixel sampling.

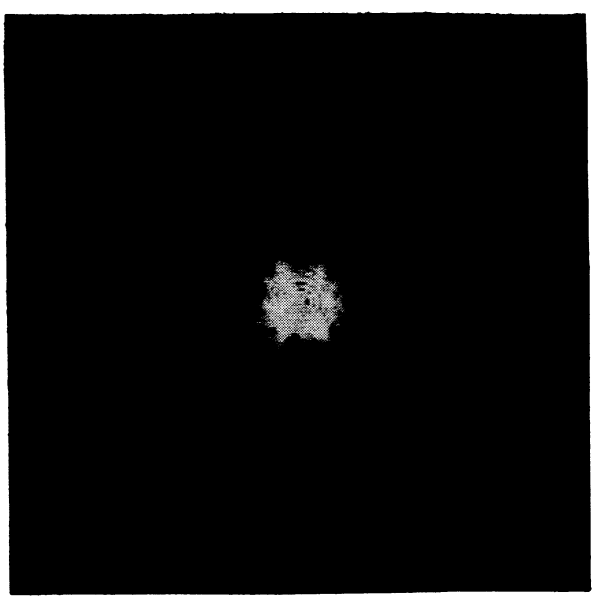

Fig. 6. Image (2) computed from the reconstructed wavefront. The 15 μm/pixel sampling is the same as in the original image shown in Fig. 5.

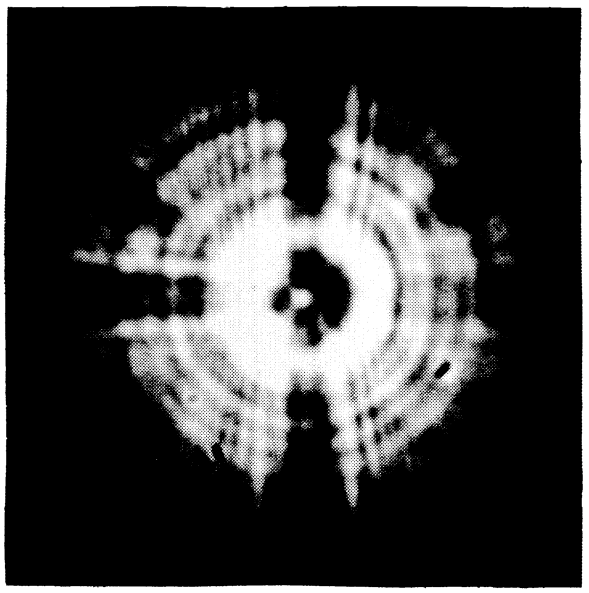

Fig. 7. Image (3) as recorded by the Space Telescope. The sampling is the original 15 μm/pixel sampling.

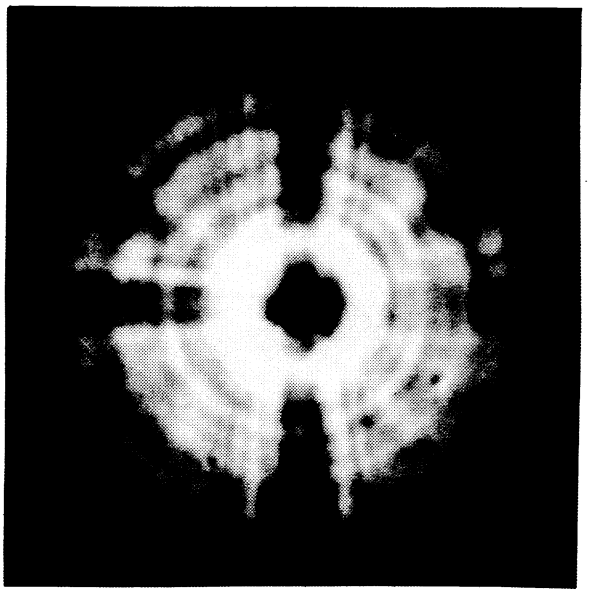

Fig. 8. Image (3) computed from the reconstructed wavefront. The 15 μm/pixel sampling is the same as in the original image shown in Fig. 7.

The results presented here were obtained by averaging all these complex amplitude estimates producing our final wavefront estimate. From this estimate one can compute the illumination in each observed image and compare the result of the computation with the actually observed illumination. This is shown in Fig. 3 to 9. Fig. 3 is the result of the computation for image (1). The 7.5 μm per pixel sampling is twice that of the observed image. The observed image is practically indistinguishable. This can be seen in Fig. 4 which shows a photometric profile across each of the two images. Fig. 5 shows image (2) as recorded by the Space Telescope. Fig. 6 is the computed image to be compared with Fig. 5. They are clearly in excellent agreement. Fig. 7 is image (3) as recorded by the Space Telescope. Fig. 8 is the computed image resampled at 15 μm per pixel for comparison with Fig. 7. The agreement is again excellent. For reference Fig. 9 shows image (3) computed from our first wavefront guess.

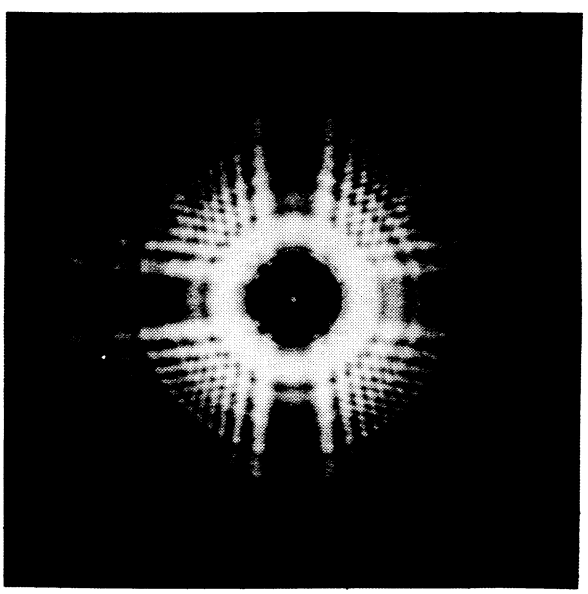

Fig. 9. Image (3) computed from the first guess. Comparison with Fig. 7 and 8 shows the improvement achieved by the phase retrieval algorithm.

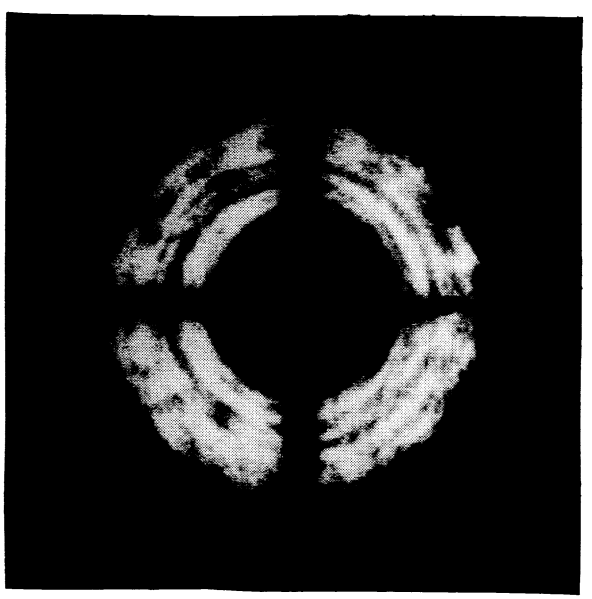

Fig. 10. Reconstructed illumination in the telescope pupil plane. Note the effect of the camera misalignment.

From the above described results it is clear that our wavefront estimate reproduces satisfactorily the observations. It should therefore also reproduce satisfactorily the illumination in the telescope pupil. Fig. 10 shows the result of the computation. The central obscuration produced by the PC camera secondary mirror is clearly seen together with the three thick supporting arms (top, bottom, and left). However they are not centered on the pupil but shifted toward the right. Since the images were taken close to the optical axis, it shows evidence for a misalignment of the PC camera. Other evidence for this misalignment was independently found by Chris Burrows [12] from images taken in the wide field (WF) configuration of the camera. It is currently attributed to a tilt of the optical prism which distributes the light to the four CCD chips. Fig. 10 also shows three of the four arms supporting the telescope secondary mirror. They are thinner than the camera arms. The fourth arm on the left is hidden behind the camera arm. The three black dots at 120° near the pupil outer edge are the three clamps holding the telescope primary mirror in place. The bottom clamp is right behind one of the telescope spider arms. The illumination on the pupil is not uniform but shows dark rings. Similar rings appear in the reconstructed wavefront map and are typical of the grooves left by a polishing tool. Because the camera entrance pupil is not conjugate to the telescope pupil and because of the additional telescope spherical aberration these grooves may diffract light outside of the camera entrance pupil thus producing the observed dark rings in the reconstructed pupil image.

The reconstructed wavefront surface shows very little aberration apart from the spherical aberration which was estimated to be 0.29 μm rms. Fig. 11 shows the residuals after removal of all the low order Zernike terms up to spherical aberration included. The white circular zone at a radius of about 0.7 pupil radius appears to be typically $\lambda/20$ above the surrounding surface and was independently found on wavefronts reconstructed from interferograms of the HST primary mirror taken prior to the launch [13]. The smaller scale rings seen on Fig. 11 may well be produced by the telescope secondary.

4. CONCLUSION

Iterative Fresnel transforms appears to be a powerful tool to test telescope optics. The technique is currently used to test millimetric antennae and was apparently applied for the first time to an optical telescope. Compared to geometrical optics methods, it produces high spatial resolution wavefront maps with images taken closer to the telescope focal plane. One disadvantage is to require quasi-monochromatic light. The spectral resolution $\lambda/\Delta\lambda$ must be of the order of the spatial resolution D/a of the reconstructed wavefront where D is the pupil diameter and a the characteristic size of the smallest wavefront perturbations which can still be resolved. A more important drawback is the limitation to small, point like sources which prevents the technique from being used on extended objects. For the HST, the quality of the wavefront reconstruction seems to be limited by the telescope jitter. Clearly the technique cannot be applied to ground-based telescopes at optical wavelength where the image is heavily blurred by the atmosphere. It looks however promising as a diagnostic tool for optical telescopes in space.

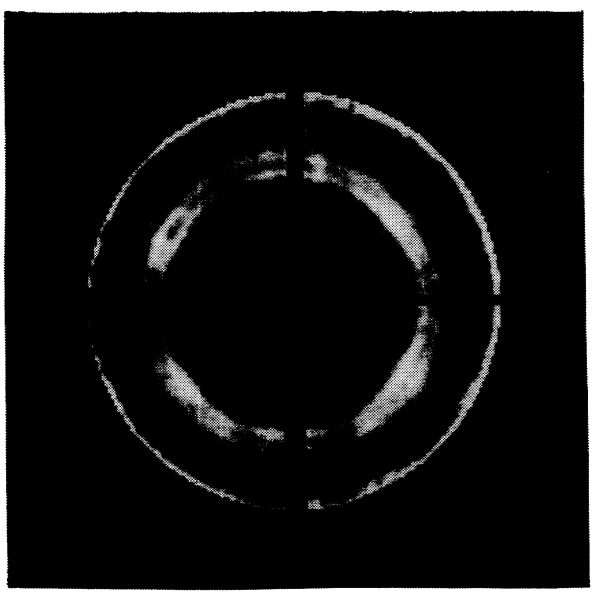

Fig. 11. Reconstructed wavefront surface after removal of all the low order aberration terms up to spherical aberration included.

5. ACKNOWLEDGEMENTS

This research has been supported in part by contract with JPL and in part by a grant from the Strategic Defense Initiative Organization, managed by the Harry Diamond Laboratories.

8. REFERENCES

[1] F. Roddier (1988), "Curvature sensing and compensation: a new concept in adaptive optics," Applied Optics **27**, 1223.

[2] F. Roddier, C. Roddier, N. Roddier (1988), "Curvature sensing: a new wavefront sensing method," SPIE **976**, 203.

[3] C. Roddier, F. Roddier, A. Stockton, A. Pickles, "Testing of telescope optics: a new approach," SPIE **1236**, 756.

[4] Gershberg R.W. and Saxton W.O. (1972), "A practical algorithm for the determination of phase from image and diffraction plane pictures," OPTIK **35**, 237.

[5] Fienup J.R. and Wackerman C.C. (1986), "Phase-retrieval stagnation problems and solutions," J. Opt. Soc. Am. A **3**, 1897.

[6] Misell D.L. (1973a), "A method for the solution of the phase problem in electron microscopy," J. Phys. D (Appl. Phys.) **6**, L6.

[7] Misell D.L. (1973b), "An examination of an iterative method for the solution of the phase problem in optics and electron optics. I: Test calculations," J. Phys. D (Appl. Phys.) **6**, 2200.

[8] Misell D.L. (1973c), "An examination of an iterative method for the solution of the phase problem in optics and electron optics. II: Sources of error," J. Phys. D (Appl. Phys.) **6**, 2217.

[9] Boucher R.H. (1980), "Convergence of algorithms for phase retrieval from two intensity distributions," SPIE **231**, 130.

[10] Morris D. (1985), "Phase retrieval in the radio holography of reflector antennas and radio telescopes," IEEE Trans. on Ant. and Prop. **AP-33**, 749.

[11] Kani L.M., Dainty J.C. (1988), "Super-resolution using the Gershberg algorithm," Opt. Commun. **68**, 11.

[12] C. Burrows (1990), Proc. of the first HARP workshop (Nov. 15-16, 1990).

[13] R. Lyon and P. Miller (1990), Proc. of the first HARP workshop (Nov. 15-16, 1990).